Chemical nonequilibrium and deconfinement in 200*A* GeV sulphur induced reactions

Jean Letessier and Johann Rafelski

Department of Physics, University of Arizona, Tucson, Arizona 85721

and Laboratoire de Physique Théorique et Hautes Energies, Université Paris 7, 2 place Jussieu, F-75251 Cedex 05, France

(Received 17 June 1998)

We interpret hadronic particle abundances produced in S-Au/W/Pb 200*A* GeV reactions in terms of the final state hadronic phase space model and determine by a data fit of the chemical hadron freeze-out parameters. Allowing for the flavor abundance nonequilibrium a highly significant fit to experimental particle abundance data emerges, which supports the possibility of strangeness distillation. We find under different strategies stable values for freeze-out temperature $T_f = 143 \pm 3$ MeV, baryochemical potential $\mu_B = 173 \pm 6$ MeV, ratio of strangeness (γ_s) and light quark (γ_q) phase space occupancies $\gamma_s/\gamma_q = 0.60 \pm 0.02$, and $\gamma_q = 1.22 \pm 0.05$ without accounting for collective expansion (radial flow). When introducing flow effects which allow a consistent description of the transverse mass particle spectra, yielding $|\vec{v}_c| = 0.49 \pm 0.01$ c, we find $\gamma_s/\gamma_q = 0.69 \pm 0.03$, $\gamma_q = 1.41 \pm 0.08$. The strange quark fugacity is fitted at $\lambda_s = 1.00 \pm 0.02$ suggesting chemical freeze-out directly from the deconfined phase. [S0556-2813(99)01402-8]

PACS number(s): 25.75.Dw, 12.38.Mh

I. INTRODUCTION

In relativistic nuclear collisions, for a short period of time, physical conditions are recreated similar to those present in the early Universe about 40 μs after the big bang. The primary objective of the extensive experimental program at BNL (Brookhaven National Laboratory) and CERN (European Organization for Nuclear Research) is the understanding of ''vacuum melting,'' the formation and properties of the deconfined quark-gluon plasma (QGP) phase of strongly interacting (hadronic) matter [1].

Our present investigation addresses the completed experimental analysis of the CERN 200*A* GeV sulphur beam reactions with laboratory stationary ''heavy'' targets, such as gold, tungsten, or lead nuclei. This highest presently available energy content materializes in form of hadronic particle multiplicity and corresponds to nuclear collisions occurring in the center of momentum frame $E_{\text{c.m.}} = \sqrt{s}/B = 8.8$ GeV $= 9.4 m_N c^2$ for each participating nucleon. Several prior attempts have been made to interpret the hadronic particle abundances and spectra within statistical particle production interpretation [2–9], and the present report takes, as we believe it, to a conclusion this extensive body of research work. The results of our present analysis are the parameters and properties of the hadronic system at chemical freeze-out. The new theoretical element which makes this attempt successful and which we introduce here is the chemical nonequilibrium abundance of light quark flavors.

This analysis of the experimental data is based on the assumption that a relatively small and dense volume of highly excited hadronic matter, the ''fireball,'' is formed in the reaction. When we speak of particle abundance freeze-out, we refer to the stage in evolution of the fireball at which density has dropped to the level that in subsequent collisions particle abundances remain unchanged. We side-step the need to understand largely unknown collective flows originating in both, the memory of the initial ''longitudinal'' collision momentum, and the explosive ''transverse'' disintegration driven by the internal pressure of the hadronic matter. Thus, all particles originate from an expanding fire-

ball surface. In order to minimize the dependence on the source shape, geometry, and dynamics, we either consider ratios of particles obtained at central rapidity, or ratios of 4π abundances. Suggestions were made that detailed production dynamics needs to be considered [8], allowing that some particles are emitted well ahead of others, and of the final state hadronization. In our approach we see evidence for at best, a two stage process, with some distillation of flavor content, and specifically strangeness leading to an *s*-quark enriched final stage. However, there is no compelling evidence for a real multistage, continuous particle production process in our evaluation of the data.

II. CHEMICAL NONEQUILIBRIUM STATISTICAL MODEL

Along with the other statistical analysis of the experimental data mentioned above, we employ the local thermal equilibrium method, and use a local freeze-out temperature T_f. One can argue that the accessibility of many degrees of freedom, as expressed by high specific entropy content, validates use of the thermal equilibrium. The usefulness of the local thermal equilibrium is, in part, based on the experimental fact that, at given transverse mass $m_\perp = \sqrt{m^2 + p_\perp^2} \simeq 1.5$–2.5 GeV, $m_\perp$ spectra of very different hadronic particles have the same inverse slope T_0 [10]. To a very adequate precision, for these high $m_\perp$, this inverse slope $T_0 \simeq 235$ MeV arises from T_f according to the Doppler blueshift relation using a local collective flow velocity. Impact of flow effects is discussed in detail in Sec. V.

Regarding chemical equilibration, we will recognize here two different types, relative and absolute [12], illustrated in the following example. Consider within a fixed volume a hot, thermally equilibrated gas of nucleons $N = p, n$, pions $\pi^\pm, \pi^0$, and Δ resonances.

Relative chemical equilibrium. The relative abundance of the *u* and *d* carrying quarks is easily established through flavor exchange reactions, such as $p + \pi^- \leftrightarrow n + \pi^0$; at the valence quark level there is no creation or annihilation process that needs to occur in each reaction to equilibrate, be-

tween the different hadronic particles, the quark flavors. We speak of relative chemical equilibration occurring through quark exchange reactions described in terms of fugacities λ_i, $i=u,d,s$. From quark fugacities, the particle fugacities are obtained, and in particular we recall that baryochemical potential arises as $\mu_B = 3T \ln \lambda_q$, where we assumed that the difference between u and d quarks is not significantly affecting the particle ratios studied here [5].

Absolute chemical equilibrium. Very much different is the process involving the equilibration between the number densities of mesons and baryons. Baryon-antibaryon formation processes are of the type $N + \bar{N} \leftrightarrow \rho + \omega$ and require that aside of the reorganization of the quark content, also the number of valance quarks changes, here between 6 and 4. The valence quark numbers have to be controlled by new parameters, the phase space occupancies γ_i, $i=u,d,s$. Only when γ_i is present can the freeze-out abundance of hadron families be differentiated.

The difference between λ_i and γ_i is that, e.g., for strange and antistrange quarks the same factor γ_s applies, while the antiparticle fugacity is inverse of the particle fugacity. The proper statistical physics foundation of γ_i is obtained considering the maximum entropy principle for evolution of physical systems. In such a study it has been determined that while the limit $\gamma_i \to 1$ maximizes the specific chemical entropy, this maximum is extremely shallow, indicating that a system with dynamically evolving volume will in general find more effective paths to increase entropy, than offered by the establishment of the absolute chemical equilibrium [11].

Generally, the microscopic processes which lead to absolute chemical equilibrium are slower than those leading to establishment of thermal or relative chemical equilibrium, considering that the inelastic reactions that change the particle abundance have usually much smaller cross section than particle number preserving exchange reaction, or elastic collisions. While thermal and relative chemical equilibrium will in general occur within the life span of dense matter formed in nuclear collisions, the approach to absolute chemical equilibrium provides interesting chronometric and structure information about the dynamics of the collision process [12,13]. In consequence, the number density of different hadrons produced in the collision has to be characterized by individual fugacities. If each hadronic species were to require its own fugacity, there would be little opportunity to relate reliably the observed particle yields to specific physical processes.

The interesting insight of this paper, concluded from the success of the description of the experimental data, is that chemical nonequilibrium is important for the understanding of the experimental results, and that there is need for just four chemical abundance parameters: two standard fugacities λ_q and λ_s (relative chemical equilibrium), and two chemical nonequilibrium occupancy parameters, measuring the abundance of valance quarks γ_s, a parameter describing the approach of strange quarks to phase space abundance equilibrium [2,12,13] and γ_q, introduced here for the first time into such data analysis, characterizing the phase space abundance of light quarks. γ_q is required as a parameter in the picture of direct hadronization of a deconfined QGP region into final state hadrons, which are free streaming and do not form an intermediate hadronic phase. When developing a dynamical description of QGP evaporation, one immediately establishes that the entropy excess we reported previously [14], requires a hadronic phase space parameter capable to control the excess of hadronic particle abundances consistently. Moreover, considering that in the fragmentation of gluons additional light quark pairs arise, and can overpopulate the phase space abundance of light quarks, we are naturally led to implement the light quark occupancy parameter γ_q. Note that such direct emission from QGP scenario, while convenient to understand the meaning of our data analysis in microscopic terms, is by far not a unique framework for the interpretation of the results we obtain. Which microscopic model is appropriate will be understood when other systems can be subject to a similar analysis as the one presented here. Comparable particle abundance data is presently assembled both for Au-Au collisions at 11A GeV at AGS-BNL, and for Pb-Pb collisions at 158A GeV at CERN, with intermediate energies available at CERN in near future.

The evaluation of the final particle yields follows the pattern established in earlier work (see, e.g., Refs. [3,5,10]). The relative number of primary particles freezing out from a source is obtained noting that the fugacity and phase space occupancy of a composite hadronic particle is expressed by its constituents and that the probability to find all j components contained within the ith emitted particle is

$$N_i \propto e^{-E_i/T} \prod_{j \in i} \gamma_j \lambda_j, \quad \lambda_i = \prod_{j \in i} \lambda_j, \quad \gamma_i = \prod_{j \in i} \gamma_j. \quad (1)$$

The unstable hadronic resonances are allowed to disintegrate and feed the stable hadron spectra. Central rapidity region $y \simeq 0$, where $E_i = \sqrt{m_i^2 + p^2} = \sqrt{m_i^2 + p_\perp^2} \cosh y$, or the full phase space coverage as required by the kinematic range of the experiments are considered. Since $p_\perp > 1$ GeV hadron spectra are not significantly deformed by decays (see Figs. 3 and 4 in Ref. [5]), one may in this limit first evaluate the partial multiplicities for different hadrons, and then allow these to decay, which speeds considerably the calculations. We have verified that this approach, which is exact for 4π multiplicities, gives results which are much more precise than the experimental uncertainties for the central $y \simeq 0$ high $p_\perp$ data, and thus we have used this approach. Once the parameters $T_f, \lambda_q, \lambda_s, \gamma_q, \gamma_s$ are determined from the particle yields available, we can characterize the entire hadronic particle phase space and obtain the physical properties of the system, such as, e.g., energy and entropy per baryon, strangeness content. Even though we are describing a free streaming gas of emitted particles, we can proceed as if we were evaluating partition function of system with the phase space distributions described by the statistical parameters, given that in a gedanken experiment we have just in an earlier moment still a cohesive, interacting system. We have implemented all relevant hadronic states and resonances in this approach and have also included quantum statistical corrections, allowing for first Bose and Fermi distribution corrections in the hadron abundances and in the phase space content. These corrections influence favorably the quality of the data fits.

Most of our analysis will be carried out within this thermochemical framework. However, in Sec. V we shall enlarge the discussion to include the analysis of $m_\perp$ particle

TABLE I. Statistical parameters obtained from fits of S-Au/W/Pb data. In fits A to D, particle abundance ratios not comprising Ω are fitted. In fits A' to D' all experimental data in Table II were used; in fits D_s and D'_s strangeness conservation in the fitted particle yields was enforced. Asterisks mean a fixed (input) value, not a parameter of the fit.

Fits	T_f [MeV]	λ_q	λ_s	γ_s	γ_q	χ^2/N_{DF}
A'	145 ± 3	1.52 ± 0.02	1^*	1^*	1^*	17
A	145 ± 3	1.52 ± 0.02	1^*	1^*	1^*	21
B'	144 ± 2	1.52 ± 0.02	0.97 ± 0.02	1^*	1^*	18
B	144 ± 2	1.53 ± 0.02	0.97 ± 0.02	1^*	1^*	22
C'	147 ± 2	1.48 ± 0.02	1.01 ± 0.02	0.62 ± 0.02	1^*	2.4
C	147 ± 2	1.49 ± 0.02	1.01 ± 0.02	0.62 ± 0.02	1^*	2.7
D'	**144 ± 3**	**1.49 ± 0.02**	**1.00 ± 0.02**	**0.73 ± 0.02**	**1.22 ± 0.06**	**0.90**
D	**143 ± 3**	**1.50 ± 0.02**	**1.00 ± 0.02**	**0.73 ± 0.02**	**1.22 ± 0.06**	**0.65**
D'_s	153 ± 3	1.42 ± 0.02	1.10 ± 0.02	0.70 ± 0.02	1.26 ± 0.06	3.04
D_s	153 ± 3	1.42 ± 0.02	1.10 ± 0.02	0.70 ± 0.02	1.26 ± 0.06	3.47

spectra, introducing the collective velocity $\vec{v}_c$. The different schemes that are possible to implement flow were studied [15]. We adopt here a radial expansion model and consider the causally disconnected domains of the dense matter fireball to be synchronized at the instance of collision — in other words the time of freeze-out is for all volume elements a common constant time in the c.m. frame. The freeze-out occurs at the surface of the fireball simultaneously in the c.m. frame, but not necessarily within a short instant of c.m. time.

Within this approach the spectra and thus also multiplicities of particles emitted are obtained replacing the Boltzmann factor in Eq. (1) by [15]

$$e^{-E_i/T} \rightarrow \frac{1}{2\pi} \int d\Omega_v \, \gamma_c (1-\vec{v}_c \cdot \vec{p}_i/E_i)$$

$$\times e^{-\gamma_c(1-\vec{v}_c \cdot \vec{p}_i/E_i)E_i/T},$$

$$\gamma_c = \frac{1}{\sqrt{1-\vec{v}_c^2}}, \tag{2}$$

a result which can be intuitively obtained by a Lorentz transformation between an observer on the surface of the fireball, and one at rest in laboratory frame. In certain details the results we obtain confirm the applicability of this simple approach.

As can be seen in Eq. (2) we need to carry out an additional two-dimensional (half-sphere) surface integral with the coordinate system fixed by an arbitrary, but fixed (collision) axis which defines the transverse particle momentum. Just a one-dimensional numerical integration over one of the surface angles needs to be carried out. To obtain the particle spectra as function of $m_\perp$ we need also to integrate over rapidity y. This rapidity integration can be approximated for a narrow rapidity interval using the error function.

III. ANALYSIS OF EXPERIMENTAL RESULTS

We now discuss the results of our data analysis. In Table I, we present ten different least square fits to the data obtained using MINUIT96.03 program from the CERN FORTRAN library. The two fits (A,A') are carried out allowing just two parameters, T_f and λ_q, leaving the remaining three chemical parameters at their implicit value ($=1$). The difference between the two fits is that A (and B,C,D) exclude data comprising the Ω yields for reasons which we will discuss momentarily. We consider here 18 data points listed in Table II (of which three comprise the Ω's) which we fit with these two parameters, thus in fit A' we have 16 and in fit A 13 degrees of freedom (N_{DF}), while in the all-parameter fits D and D' we have 13 and respectively 10 N_{DF}. As seen by the large χ^2/N_{DF} shown in last column of Table I, the fit A is not acceptable. Moreover, fitting λ_s (fits B,B'), and thus in effect testing the so-called hadronic gas model [4], is actually not improving the validity of the description, even though we have not enforced here the strangeness conservation among the emitted hadrons. Setting $\langle s-\bar{s}\rangle=0$ introduces a constraint between the 3 parameters which is difficult to satisfy. Implementing such strangeness conservation (not shown in Table I) we find that the fit to all data has $\chi^2/N_{DF}\simeq24$, with 16 N_{DF}.

In short, the equilibrium hadron gas model of particle production fails today to describe the precise experimental particle abundances, our finding contradicts strongly earlier expectations [6]. The major discrepancies, as shown in Table II column B, include Ξ/Λ [10 standard deviations (SD) and 7 SD], $\bar{\Xi}/\bar{\Lambda}$ (6 SD), $K_s^0/\bar{\Lambda}$ (5 SD). Two values of same particle ratios appear here since if a particle ratio is available at fixed $p_\perp$ and fixed $m_\perp$, both are fitted and the total χ^2 included in analysis, as these experimental results correspond to different data samples. We did not include in our analysis the same data sample as seen in Ref. [6], but the number of degrees of freedom remains similar. We have introduced precision central rapidity strange baryon and antibaryon results, and omitted several results (see below) that we could not consider as having a straightforward thermal interpretation. We do not see our data selection as biased, as in the end we are retaining a quite diverse sample typically with smallest errors. We did not consider the NA44 deuteron yields since it is difficult to distinguish the direct, thermally produced fraction from final state interaction formation (and depletion), η/π^0 of WA80 as the flavor evolution of the η has not been fully understood within the thermal model,

TABLE II. Available particle ratios: experimental results for S-W/Pb/Au, references for the results in second column, momentum or transverse mass cuts (in GeV) in third column, followed by columns showing the different fits, corresponding to those in Table I. Asterisks mean a predicted result (corresponding data is not fitted).

Ratios	Ref.	Cuts	Data	Fit A	Fit B	Fit C	**Fit D**	**Fit D$'$**	Fit D_s	Fit D'_s
Ξ/Λ	[17]	$1.2<p_\perp<3$	0.097 ± 0.006	0.162	0.157	0.105	**0.099**	**0.100**	0.110	0.111
$\bar\Xi/\bar\Lambda$	[17]	$1.2<p_\perp<3$	0.23 ± 0.02	0.36	0.38	0.23	**0.22**	**0.22**	0.18	0.18
$\bar\Lambda/\Lambda$	[17]	$1.2<p_\perp<3$	0.196 ± 0.011	0.194	0.202	0.205	**0.203**	**0.203**	0.203	0.203
$\bar\Xi/\Xi$	[17]	$1.2<p_\perp<3$	0.47 ± 0.06	0.43	0.48	0.44	**0.45**	**0.44**	0.33	0.33
$\bar\Omega/\Omega$	[18]	$p_\perp>1.6$	0.57 ± 0.41	1.00*	1.18*	0.96*	**1.01***	**0.98**	0.55*	0.55
$\dfrac{\Omega+\bar\Omega}{\Xi+\bar\Xi}$	[18]	$p_\perp>1.6$	0.80 ± 0.40	0.27*	0.27*	0.17*	**0.16***	**0.16**	0.16*	0.16
K^+/K^-	[17]	$p_\perp>0.9$	1.67 ± 0.15	1.96	2.06	1.78	**1.82**	**1.80**	1.43	1.43
K_s^0/Λ	[19]	$p_\perp>1$	1.43 ± 0.10	1.51	1.56	1.64	**1.41**	**1.41**	1.25	1.25
$K_s^0/\bar\Lambda$	[19]	$p_\perp>1$	6.45 ± 0.61	7.85	7.79	8.02	**6.96**	**6.96**	6.18	6.17
K_s^0/Λ	[17]	$m_\perp>1.9$	0.22 ± 0.02	0.26	0.26	0.28	**0.24**	**0.24**	0.24	0.24
$K_s^0/\bar\Lambda$	[17]	$m_\perp>1.9$	0.87 ± 0.09	1.33	1.30	1.38	**1.15**	**1.16**	1.20	1.20
Ξ/Λ	[17]	$m_\perp>1.9$	0.17 ± 0.01	0.28	0.27	0.18	**0.17**	**0.17**	0.18	0.18
$\bar\Xi/\bar\Lambda$	[17]	$m_\perp>1.9$	0.38 ± 0.04	0.62	0.64	0.38	**0.38**	**0.37**	0.30	0.30
$\dfrac{\Omega+\bar\Omega}{\Xi+\bar\Xi}$	[17]	$m_\perp>2.3$	1.7 ± 0.9	0.95*	0.98*	0.59*	**0.58***	**0.58**	0.52*	0.52
$p/\bar p$	[20]	midrapidity	11 ± 2	11.0	11.2	10.1	**10.6**	**10.5**	7.96	7.96
$\bar\Lambda/\bar p$	[21]	4π	1.2 ± 0.3	2.43	2.50	1.47	**1.44**	**1.43**	1.15	1.15
$\dfrac{h^-}{p-\bar p}$	[22]	4π	4.3 ± 0.3	4.5	4.4	4.2	**4.1**	**4.1**	3.6	3.6
$\dfrac{h^+-h^-}{h^++h^-}$	[23]	4π	0.124 ± 0.014	0.109	0.114	0.096	**0.103**	**0.102**	0.092	0.092

$\phi/(\rho+\omega)$ of NA34 (Helios 3) as it is obtained in the forward rapidity domain and thus subject to considerable flow influence not studied in detail here, the early NA44 pion to nucleon ratios were used in [6], but these are obtained from nonoverlapping rapidity regions, and data was not corrected for the weak hyperon feed down decay. However, we considered that it is very important to include a similar data sample in the fit, as the pion to nucleon ratio is strongly temperature dependent (see below Fig. 3). However, the results from NA35 are available only for S-Ag reactions, a somewhat lighter collisions system. We have looked carefully at the systematics of these and other results offered by the NA35/49 Collaboration and have determined that the ratio $h^-/(p-\bar p)$ ($h^\pm$ are all positively or negatively charged hadrons) shows little variability between the different systems studied. In S-S the result is 4.6 ± 0.4, in S-Ag (see Table II) it is 4.3 ± 0.3 and in Pb-Pb it is 4.4 ± 0.5, see Ref. [9] for data review. We thus adopted in our fit the central value observed in S-Ag collisions. The smallest error we chose is a conservative assumption here, as it in principle pushes the overall error of the fit up. In passing we also note that another related variable we consider here in difference to earlier work [5], is the ratio $(h^+-h^-)/(h^++h^-)$. We fit now the 4π data of EMU05, rather than the central pseudorapidity domain value.

In the fits (C,C'), we introduce γ_s, i.e., strangeness chemical nonequilibrium is allowed for [2]. This single parameter reduces greatly χ^2/N_{DF}, which drops by a factor 10, providing a major improvement in comparison between theory and experiment. The resulting fit is fully compatible with the scenario **B** in Ref. [5]. However, presence of additional and/or more precise experimental data makes this fit, which was five years ago possible, now statistically also not acceptable. For $18-4=14$ N_{DF} (fit C' including Ω's), $\chi^2/N_{DF}=2.4$ is expected to arise in less than 1% of experiments. Clearly some physics is missing in this description of the data. It has been argued that a more refined dynamical particle production model is needed to account for this discrepancy, reflecting on some complex dynamics involved in particle production (see, e.g., Ref. [8]). The surprise is that all that is needed is the chemical nonequilibrium of the light quark abundance.

We now introduce γ_q. The full fit to all data (fit D') is statistically significant, with $\chi^2/N_{DF}=0.9$. The profile of χ^2/N_{DF} as function of T_f shown in Fig. 1 (thin solid line) shows a well defined minimum at 144 ± 3 MeV. We note, in passing, that quite different considerations have led others to propose a universal chemical freeze-out temperature at nearly exactly this value [16]. The thick solid line in Fig. 1 (fit D) arises when, in the fit, one excludes three data points involving completely strange Ω's. We came to try this, since when exploring the stability of the fit D' against suppression of some of the data, we noted that the fit D as expressed by χ^2/N_{DF} is better. As can be seen in Fig. 1, the fit D minimum
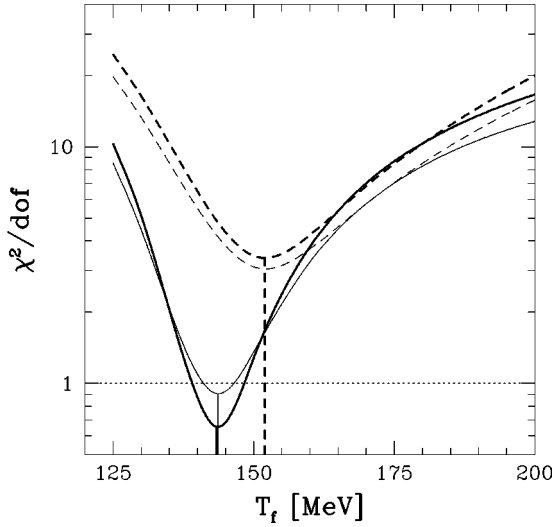
FIG. 1. χ^2/N_{DF} profile as function of temperature for the chemical nonequilibrium fits: without strangeness conservation constraint D (thick solid line), D' (thin solid line), and with strangeness conservation constraint D_s (thick dashed line), D'_s (thin dashed line). Thick lines exclude the three Ω-data points.

(thick solid line at $T_f = 143$ MeV) is sharper and χ^2/N_{DF} drops to 0.65. In the Table I, we further see that the removal of these three data points has for all the other fits the effect of reducing the significance of the fit, as would be expected given the few degrees of freedom we have at our disposal. That an improvement occurs when the fit is statistically significant signals that there is probably an additional mechanism of Ω formation contributing to the yields. This indeed is what we expect, since we have not enforced the strangeness conservation in the fits D (in boldface) and D' shown in Table I. Enforcing strangeness conservation leads to fits denoted (D_s, D'_s) with $\chi^2/N_{DF} > 3$, and thus not offering an acceptable interpretation of the data. There indeed is also not a well defined χ^2 minimum in the associated distributions shown by dashed lines in Fig. 1.

Thus the following simple reaction scenario emerges: in the particle evaporation-dissociation process at $T_f = 143 \pm 3$ MeV there is predominant emission of $\bar{s}$-carrying hadrons (see below) leading to an s-carrier rich residue that populate lower $p_\perp$ kaon and hyperon yields that remained not fully measured. It should be stressed here that the data we fit are very sparse in the small $p_\perp < 1$ GeV domain, thus an imbalance between $\bar{s}$ and s we show in Table III, simply

should be read to mean that the opposite imbalance is to be expected for soft hadrons. A soft hadron excess arising from disintegration of s-quark enriched residue becomes particularly visible in the Ω abundance, since the abundance of these particles is small, while their production by strangeness rich source is probably enhanced, speaking here in relative terms. We note that such strangeness distillation has been foreseen to occur [24], and specifically in this manner if QGP phase hadronizes at temperatures found in our fits of the data [25]. This dynamical distillation process stimulated several searches for strangelets, i.e., (quasi) stable highly strange hadrons with more than three strange quarks [26,27].

IV. PROPERTIES OF HADRONIC PARTICLE PHASE SPACE

Given the precise statistical information about the hadron phase space provided by the fit D, we can determine the specific content in energy, entropy, strangeness carried out by hadronic particles, see Table III. For each fit we show the chemical freeze-out temperature T_f, the hadron phase space properties: specific (per baryon) energy, entropy, (anti)strangeness, strangeness imbalance, and the freeze-out pressure P_f and volume V_f. The specific $\bar{s}$ content is determined to be 0.90 ± 0.04. We find that there is an excess of $\bar{s}$-carrying hadrons carried away at higher $p_\perp$. The specific entropy content 48.2 ± 3 of the best fit D, agrees well with the evaluation made earlier [14]. This is so because the fit of predominantly high $p_\perp$ strange particle data is fully consistent with the 4π total multiplicity results. The pressure of the hadronic phase space $P_f = 82 \pm 6$ MeV/fm^3 has the magnitude of the vacuum confinement pressure. If the chemical freeze-out were the result of a disintegration after QGP expansion to the point of instability into volume fragmentation, this would be according to the Gibbs criterion the transformation pressure. In that case our fit amounts to the measurement of the confinement pressure (bag constant $\mathcal{B}$). The volume V_f we quote arises by assuming that the hadronic phase space comprises for the S-W collisions baryon number $B = 120$. It implies in the case of fit D a hadron phase space energy density $\epsilon_f = 0.43 \pm 0.4$ GeV/fm^3. Both, V_f and ϵ_f have physical meaning only if the chemical freeze-out occurs nearly simultaneously within the entire body of the source.

The energy per baryon found in emitted hadronic particles is remarkably consistent with the expectation based on kinematic energy content, should the deposition of energy and baryon number in the fireball be identical [28]. For the fa-

TABLE III. T_f and physical properties of the full hadron phase space characterized by the statistical parameters given in Table I.

| Fits	T_f [MeV]	E_f/B	S_f/B	$\bar{s}_f/B$	$(\bar{s}_f - s_f)/B$	P_f [GeV/fm^3]	V_f [fm^3]
A	145 ± 3	9.01 ± 0.50	50.1 ± 3	1.64 ± 0.06	0.37 ± 0.02	0.056 ± 0.005	3352 ± 350
B	144 ± 2	8.89 ± 0.50	50.0 ± 3	1.66 ± 0.06	0.44 ± 0.02	0.056 ± 0.005	3343 ± 350
C	147 ± 2	9.25 ± 0.50	48.5 ± 3	1.05 ± 0.05	0.23 ± 0.02	0.059 ± 0.005	3529 ± 350
D	**143 ± 3**	**9.05 ± 0.50**	**48.2 ± 3**	**0.91 ± 0.04**	**0.20 ± 0.02**	**0.082 ± 0.006**	**2524 ± 250**
D$'$	**144 ± 2**	**9.07 ± 0.50**	**48.3 ± 3**	**0.91 ± 0.05**	**0.20 ± 0.02**	**0.082 ± 0.006**	**2521 ± 250**
D_s	153 ± 3	8.89 ± 0.50	45.1 ± 3	0.76 ± 0.04	0^*	0.133 ± 0.008	1520 ± 150
D'_s	153 ± 3	8.87 ± 0.50	45.1 ± 3	0.76 ± 0.05	0^*	0.134 ± 0.008	1515 ± 150
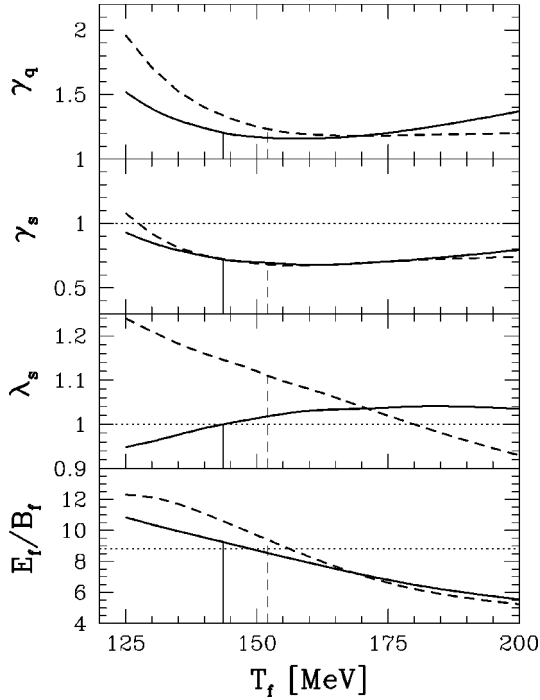
FIG. 2. Variation of $E_f/B_f, \lambda_s, \gamma_s$, and γ_q as function of temperature T_f, with all other parameters fixed by least square fit to the data.

FIG. 3. Variation of $h^-/(p-\bar{p})$ as function of T_f for fits D (solid line) and strangeness conserving D_s (dashed line). Vertical lines point to best fit location, horizontal dotted lines brace the experimental result (see Table II).

vored fit D, we find $E_f/B = 9.05 \pm 0.5$ GeV, to be compared with kinematic value 8.8 GeV obtained for central collision of sulphur with a tube of matter in the larger target. Moreover, the different fits cross the kinematic value (dotted horizontal line in Fig. 2, bottom portion) very near to best fit temperatures. The computed values of E_f/B are shown in Fig. 2 for a given T_f for fit D (solid line, no Ω or strangeness conservation) and fit D_s (dashed line, no Ω, with strangeness conservation), with all the other parameters obtained from a least square fit at given temperature. The locations of the best χ^2/N_{DF} are indicated by vertical lines. In the second section from the bottom in Fig. 2, we draw attention to another remarkable physical result of the fit D: the value $\lambda_s = 1.00 \pm 0.02$ suggests as the source of these particles a state symmetric between s and $\bar{s}$ quarks, naively expected in the deconfined phase. It is not an accident, and we could have easily found another result, since λ_s varies as function of fitted T_f.

The nonequilibrium parameters, shown in the top two sections of Fig. 2, are opening the minimum in the χ^2/N_{DF} distribution shown in Fig. 1, without a major dislocation in the parameter space as is seen in Table I. The result of interest here is that both consistently differ from their equilibrium values $\gamma_s = 1$, $\gamma_q = 1$. The values $\gamma_s = 0.73 \pm 0.02$ and $\gamma_q = 1.22 \pm 0.06$ are compatible with the physics based expectations: the computed rate of strangeness production in the deconfined phase is suggestive of this result which is noticeably below the full phase space equilibration [10,13]. Fragmentation of remaining gluons at $T_f = 143$ MeV naturally leads to the value of γ_q we obtain. As shown in the top half of Fig. 2, for the entire range of freeze-out temperature of physical interest, the values of γ_s and γ_q vary somewhat, but consistently remain in the physical domain described
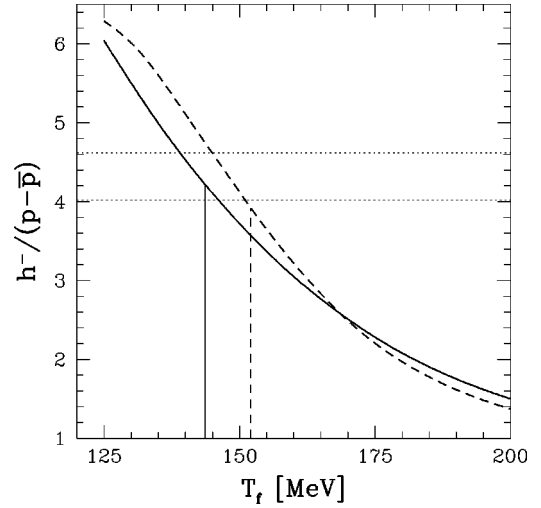
above, and are similar for fits with and without strangeness conservation. Even a short view of Fig. 2 shows that strangeness conservation condition, which introduces the greatest systematic uncertainty into this study, is capable to influence the value of λ_s, but not the chemical nonequilibrium parameters shown in Table I, or other interesting properties of the hadron source displayed in Table III.

The sensitivity of the computed specific negative hadron yield to the freeze-out temperature T_f is shown in Fig. 3. For a given value of T_f all the other parameters follow values determined by least square fit. The solid line is for fit D, dashed line for strangeness conserving fit D_s. Vertical lines are indicating the location of the best fits, horizontal dotted lines show the range of the NA35-experimental result for S-Ag collisions. The result shown in Fig. 3 makes it clear that it is impossible to consider chemical freeze-out to occur outside of the temperature window $135 < T_f < 155$ MeV. Our use of all accessible experimental particle production data in S-Au/W/Pb reactions eliminates thus from further consideration the recent suggestion of hadronic particle production universality between $e^+ + e^-$, $p + \bar{p}$, $p + p$, $A + A$ reactions with chemical freeze-out at $T_f \simeq 180$ MeV [9]. In our view, it is more natural to see earlier (i.e., higher T_f) chemical freeze-out in light collision systems, as compared to heavy ion collisions. We note that in Ref. [9], as here, the chemical freeze-out conditions are studied, and that subsequent to establishment of particle abundances there could still be particle number conserving (elastic) evolution of the hadronic matter to the point of full decoupling at a lower temperature. During this evolution the final shape of the particle spectra is determined. Thus data fits based on details of particle spectra, in particular including the low $m_\perp$, are geared to yield a thermal freeze-out temperature T_{th} that is yet lower than our T_f [29].

V. IMPACT OF COLLECTIVE FLOW ON FREEZE-OUT PROPERTIES

So far we have considered only the particle yields, and have not addressed particle spectra which, as mentioned in

the beginning of Sec. II, requires that we allow for the Doppler-like blueshift of the particles emitted from a moving source at hadronization. To do this we need to explicitly add to the least square fit another parameter, the collective velocity $\vec{v}_c$. While the integral over the entire phase space of the flow spectrum yields as many particles with and without flow, when acceptance cuts are present particles of different mass experience differing flow effects. We consider here the radial flow model, perhaps of the simplest of the complex flow cases possible [15], but it suffices to fully assess the impact of flow on our analysis.

For given pair of values T_f and v_c, the resulting $m_\perp$ particle spectrum is obtained and analyzed using the shape and procedure employed by the experimental groups, and the inverse slope ''temperature'' T_s^j is determined for each particle j — since we have the experimental results for T_s^j, we can indeed include these in our data fit. v_c is thus just one additional parameter and there are in principle several new data points available. However, in consideration of their similarity [30], with values overlapping within error, we decided to include in the chemical fit only one value $T_s = 235 \pm 10$, chosen near to the value of most precise Λ spectra. Once the chemical fit yields T_f and v_c, we check how other particles have fared. The resulting T_s^j are in remarkable agreement with experiment, well beyond what was fitted: we find for kaons, lambdas, and cascades the values $T_s^j = 215$, 236, and 246 MeV, respectively, which both in trend and value agrees with the $K^0, \Lambda, \bar{\Lambda}, \Xi$, and $\bar{\Xi}$ WA85 results [30]: $T_s^{K^0} = 219 \pm 5$, $T_s^\Lambda = 233 \pm 3$, $T_s^{\bar{\Lambda}} = 232 \pm 7$, $T_s^\Xi = 244 \pm 12$, and $T_s^{\bar{\Xi}} = 238 \pm 16$.

Since the flow effect shifts particles of different mass differently into different domains of $m_\perp, y$, it is not surprising that the inclusion of flow only impacts the phase space abundance parameters, beyond the errors of the fits. The fit D remains the best, it has now $\chi^2/N_{DF} = 0.73$, and the parameter values we gave in abstract. Fit D' has $\chi^2/N_{DF} = 0.83$. In order to facilitate comparison with other work we note that to greater precision our fit D with flow yields $T = 142.7 \pm 2.1$ MeV, $\mu_b = 176 \pm 3$, and $v_c = 0.486 \pm 0.010$ c. The situation with strangeness nonconservation remains unchanged, both fits D_s and D_s' have negligible confidence level with $\chi^2/N_{DF} \simeq 3.2$. The strangeness imbalance in fits D, D' is the same as we have obtained without flow. Thus this imbalance is not result of flow effects, but is an intrinsic property of the evolution of the fireball. An interesting feature of with flow fit is that there is little correlation between now six parameters in the fit, in other words the flow velocity is a truly new degree of freedom in description of the experimental data. We checked that nearly the same flow velocity is found when we disregard in the fit the experimental inverse slope. It is for this reason that we present here the simple radial flow model, as within this scheme the inverse transverse slope of hadrons is correctly ''predicted'' by the chemical freeze-out analysis with flow. We note that in just one aspect the fits with flow offer a new insight: the value of γ_s we obtained is compatible with unity. This value was noted already in the fit of the S-S collision results [31], and so far eluded the analysis of S-W/Au/Pb collisions.

With $\gamma_q^2 \simeq 2$ the analysis of excess entropy production

[14] is fully confirmed, and indeed in fit D with flow the entropy per baryon is 46.3, within the bounds shown in Table III. The energy content in the phase space is slightly different: the intrinsic energy per baryon at freeze-out is $E/B = 8.55$ GeV, which when multiplied with the factor γ_c reaches $E/B = 9.78$ GeV. The freeze-out pressure $P_f = 0.123$ GeV/fm^3, roughly growing with a power of γ_q, has accordingly increased.

As this discussion has shown, the analysis of particle abundances and spectra has to be combined in order to be certain that all the physical parameters acquire their true value. Even though there is still considerable uncertainty about other freeze-out flow effects, such as longitudinal flow (memory of the collision axis), the level of consistency and quality of our fit suggests that for the observables considered here these effects do not matter. Considering the quality of the data description obtained using the chemical nonequilibrium parameters, it is impossible to classify results presented here as accidental and likely to see further major revision.

In conclusion, we have here shown that the hard ($p_\perp > 1$ GeV) strange particle production data, combined with the global hadron multiplicity (entropy), can be consistently interpreted within a picture of a hot hadronizing blob of matter governed by statistical parameters acquiring values expected if the source structure is that of deconfined QGP. We have shown that the radial flow allows to account exactly for the difference between chemical freeze-out temperature $T_f = 143$ MeV and the observed $m_\perp$ spectral shape having an inverse $m_\perp$ slope $T_s = 235 \pm 10$, and thus allows a full description of kaon, baryon, and antibaryon spectra. We find a highly significant fit to experimental data, with a source characterized by $\lambda_s = 1$, specific baryon energy $E/B \simeq 9$ GeV, and high specific entropy $S/B \simeq 50$. The dense blob of matter was expanding with a surface velocity $v_c \simeq 0.49$ c. The near equilibrium abundance of strange quarks ($\gamma_s \simeq 1$, including flow), and the overabundance of light quarks ($\gamma_q^2 \simeq 2$), is pointing to a deconfined, fragmenting quark-gluon fireball as the direct particle emission source. At freeze-out we find the particle phase space pressure $P_f \simeq 0.1$ GeV/fm^3, which may be interpreted as the pressure needed to overcome the external vacuum pressure (bag constant $\mathcal{B}$). Strangeness nonconservation at high $p_\perp$ seen in our fit favors an evolution scenario in which the process of hadronization into hard particles enriches by distillation the fireball remnant with strangeness content. Given an excess of $\bar{s}$ emission at high $p_\perp$ of 0.2 strange particles per baryon, we expect at small $p_\perp$ a non-negligible 20% excess of s carriers over $\bar{s}$ carriers, potentially helping the formation of strange quark matter nuggets. The lessons learned in this study will likely prove helpful in the forthcoming interpretation of the Pb-Pb data, and the future RHIC-BNL data analysis.

Note added in proof. A similar analysis of the Pb-Pb 158A GeV collision system has been completed [32] and a comparison with the here presented S-A results, including flow, is also in press [33].

[1] J. W. Harris and B. Müller, Annu. Rev. Nucl. Sci. **46**, 71 (1996), and references therein.

[2] J. Rafelski, Phys. Lett. B **262**, 333 (1991); Nucl. Phys. **A544**, 279c (1992).

[3] J. Letessier, A. Tounsi, and J. Rafelski, Phys. Lett. B **292**, 417 (1992); hep-ph/9711351; J. Rafelski, J. Letessier, and A. Tounsi, Dallas–ICHEP, 1992, Report No. QCD161:H51:1992, hep-ph/9711350, p. 983.

[4] E. Suhonen, J. Cleymans, K. Redlich, and H. Satz, in Proceedings of the International Europhysics Conference on High Energy Physics, Marseilles, France, 1993, Marseilles EPS HEP, 1993, Report No. QCD161:I48:1993, hep-ph/9310345, p. 519.

[5] J. Letessier, A. Tounsi, U. Heinz, J. Sollfrank, and J. Rafelski, Phys. Rev. D **51**, 3408 (1995), and references therein; hep-ph/9212210.

[6] P. Braun-Munzinger, J. Stachel, J. P. Wessels, and N. Xu, Phys. Lett. B **365**, 1 (1996).

[7] J. Sollfrank, J. Phys. G **23**, 1903 (1997).

[8] F. Grassi and O. Socolowski, Jr., Phys. Rev. Lett. **80**, 1170 (1998).

[9] F. Becattini, M. Gazdzicki, and J. Sollfrank, Eur. Phys. J. C **5**, 143 (1998).

[10] J. Rafelski, J. Letessier, and A. Tounsi, Acta Phys. Pol. B **27**, 1035 (1996), and references therein.

[11] J. Letessier, A. Tounsi, and J. Rafelski, Phys. Rev. C **50**, 406 (1994); J. Rafelski, J. Letessier, and A. Tounsi, Acta Phys. Pol. A **85**, 699 (1994).

[12] P. Koch, B. Müller, and J. Rafelski, Phys. Rep. **142**, 167 (1986).

[13] J. Rafelski and B. Müller, Phys. Rev. Lett. **48**, 1066 (1982); **56**, 2334(E) (1986).

[14] J. Letessier, A. Tounsi, U. Heinz, J. Sollfrank, and J. Rafelski, Phys. Rev. Lett. **70**, 3530 (1993).

[15] E. Schnedermann, J. Sollfrank, and U. Heinz, in *Particle Production in Highly Excited Matter*, Vol. 303 of NATO *Advanced Study Institute Series B: Physics*, edited by H. H. Gutbrod and J. Rafelski (Plenum, New York, 1993), pp. 175–206.

[16] Nu Xu, for the NA44 Collaboration, I. G. Bearden *et al.*, Nucl. Phys. **A610**, 175c (1996).

[17] S. Abatzis *et al.*, WA85 Collaboration, Heavy Ion Phys. **4**, 79 (1996).

[18] S. Abatzis *et al.*, WA85 Collaboration, Phys. Lett. B **347**, 158 (1995).

[19] S. Abatzis *et al.*, WA85 Collaboration, Phys. Lett. B **376**, 251 (1996).

[20] I. G. Bearden *et al.*, NA44 Collaboration, Phys. Rev. C **57**, 837 (1998).

[21] D. Röhrich for the NA35 Collaboration, Heavy Ion Phys. **4**, 71 (1996).

[22] The S-Ag value is adopted here: T. Alber *et al.*, NA35 Collaboration, Eur. Phys. J. C **2**, 643 (1998).

[23] A. Iyono *et al.*, EMU05 Collaboration, Nucl. Phys. **A544**, 455c (1992); Y. Takahashi *et al.*, EMU05 Collaboration (private communication).

[24] C. Greiner, P. Koch, and H. Stocker, Phys. Rev. Lett. **58**, 1825 (1987).

[25] J. Rafelski, Phys. Lett. B **190**, 167 (1987).

[26] T. A. Armstrong *et al.*, E864 Collaboration, Nucl. Phys. **A625**, 494 (1997); Phys. Rev. Lett. **79**, 3612 (1997).

[27] G. Appelquist *et al.*, NA52 Collaboration, Nucl. Phys. **A566**, 507c (1994); Phys. Rev. Lett. **76**, 3907 (1996).

[28] J. Letessier, A. Tounsi, and J. Rafelski, Phys. Lett. B **333**, 484 (1994).

[29] J. R. Nix, D. Strottman, H. W. van Hecke, B. R. Schlei, J. P. Sullivan, and M. Murray, in *Advances in Nuclear Dynamics*, edited by W. Bauer and G. Westfall (Plenum, New York, in press), Vol. 3, nucl-th/9801045.

[30] D. Evans for the WA85 Collaboration, Heavy Ion Phys. **4**, 79 (1996).

[31] J. Sollfrank, M. Gaździcki, U. Heinz, and J. Rafelski, Z. Phys. C **61**, 659 (1994).

[32] J. Letessier and J. Rafelski, hep-ph/9807346, Acta Phys. Pol. B (in press).

[33] J. Letessier and J. Rafelski, hep-ph/9810332, J. Phys. G (in press).